**Electronic Supplementary Material**

Improving Molecular Alignment and Charge Percolation in Semiconducting Polymer Films with Highly Localized Electronic States through Tailored Thermal Annealing

Alessandro Luzio,[*a] *Jaime Martin,*[b,c,d] *Christina H. Cheng,*[e] *Natalie Stingelin,*[f,g] *Michael F. Toney,*[h] *Alberto Salleo* [e] *and Mario Caironi* [*a]

a.   Center for Nano Science and Technology@PoliMi, Istituto Italiano di Tecnologia, Milano 20133, Italy.

b.   POLYMAT University of the Basque Country UPV/EHU, Paseo Manuel de Lardizabal 3, Donostia-San Sebastián, 20018, Spain.

c.   Ikerbasque Basque Foundation for Science, Bilbao, 48013, Spain.

d.   Universidade da Coruña, Grupo de Polímeros, Campus de Esteiro, 15403, Ferrol, Spain.

e.   Stanford University, Department of Materials Science and Engineering, Stanford, CA, 94305 USA.

f.   School of Materials Science and Engineering and School of Chemical & Biomolecular Engineering, Georgia Institute of Technology, 311 Ferst Drive, Atlanta, GA, 30332 USA.

g.   Laboratoire de Chimie des Polymères Organiques–LCPO, UMR5629 Universitéde Bordeaux, Allée Geoffroy Saint Hilaire, Bâtiment B8 CS50023, Pessac Cedex, 33615 France.

h.   Department of Chemical and Biological Engineering, University of Colorado Boulder, Boulder, CO 80309 USA.

Table S1. Molecular weight distribution as extracted with high temperature GPC (trichlorobenzene) and thermal properties as extracted from DSC reported in Figure S1 of the PNDI-T2 derivatives of this work.
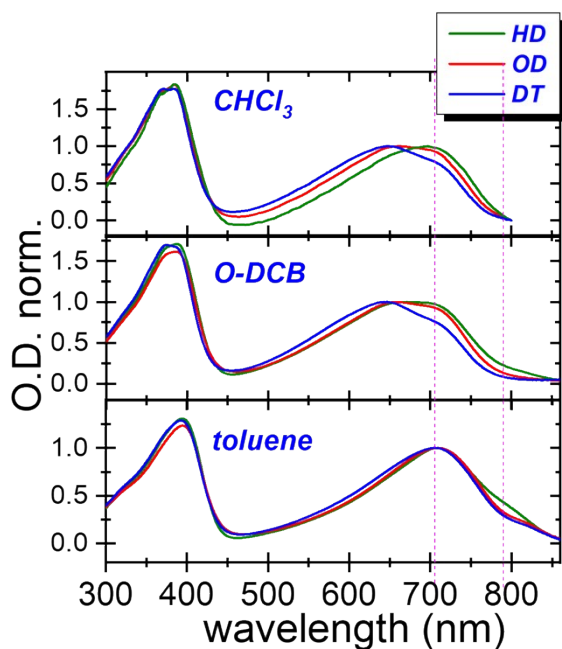
| Polymer	M_w (kg/mol)	PDI	ΔH_m, ΔH_f (kJ/mol)
DT	91.3	2.8	7.91, 3.64
OD	85.2	3.2	5.96, 5.59
HD	55.4	3.3	18.93, 14.28
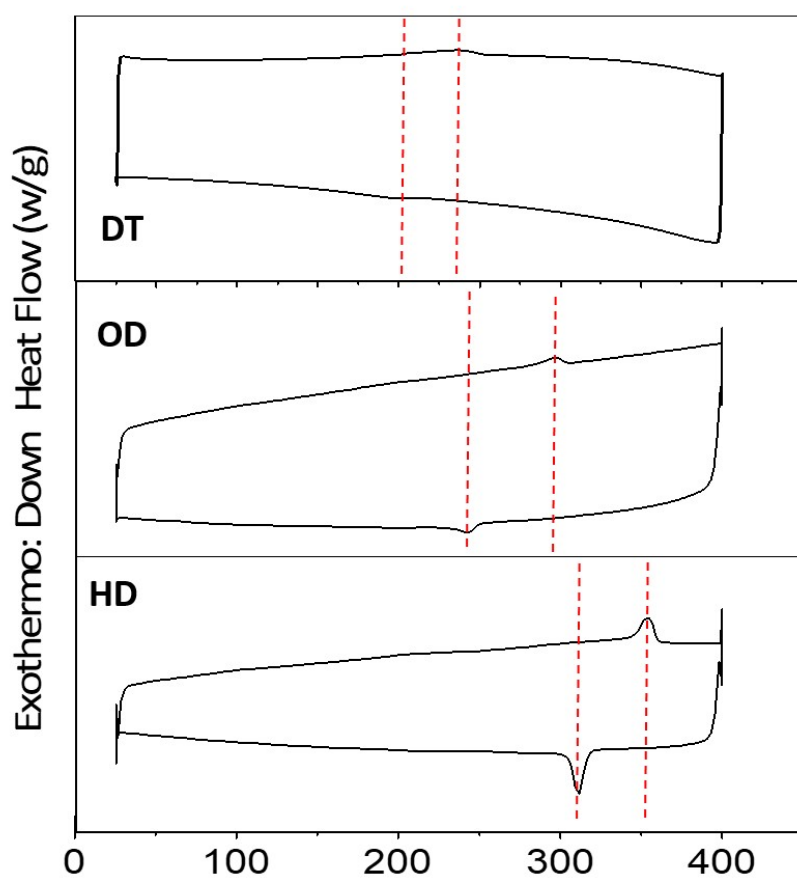
***Figure S1.*** DSC of PNDI-T2 materials
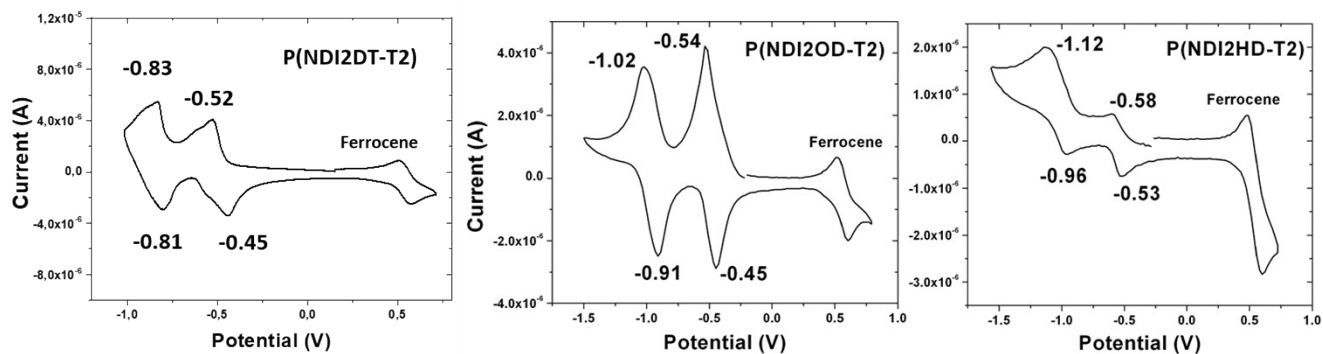
**Figure S2.** Cyclic voltammograms of PNDI-T2 as thin-films.

Figure S3. Optical absorption spectra of diluted (0.1 g/l) solutions of PNDI-T2 derivatives. The bands peaking at $\lambda \approx 700$ nm and $\lambda \approx 775$ nm are acknowledged solution aggregation optical markers.[1] In case of OD and DT the solvent inducing the highst content of aggregates is Toluene; for this reason we selected Toluene as the solvent for the ink formulations of this work (5 g/l to obtain 30 nm – 50 nm thick films).[2] Regarding HD derivative, 1,2-dichlorobenzene and Toluene induce high aggregates content, however solubility is too limited for effective thin films processing. Nevertheless, solution aggregation mechanism is already effective in Chloroform, in which high enough polymer dilution is allowed (5 g/l to obtain 30 nm – 50 nm thick films). For this reason, despite Chloroform does not induce the highest concentration of aggregates, it has been selected as the solvent for the HD ink formulations of this work.
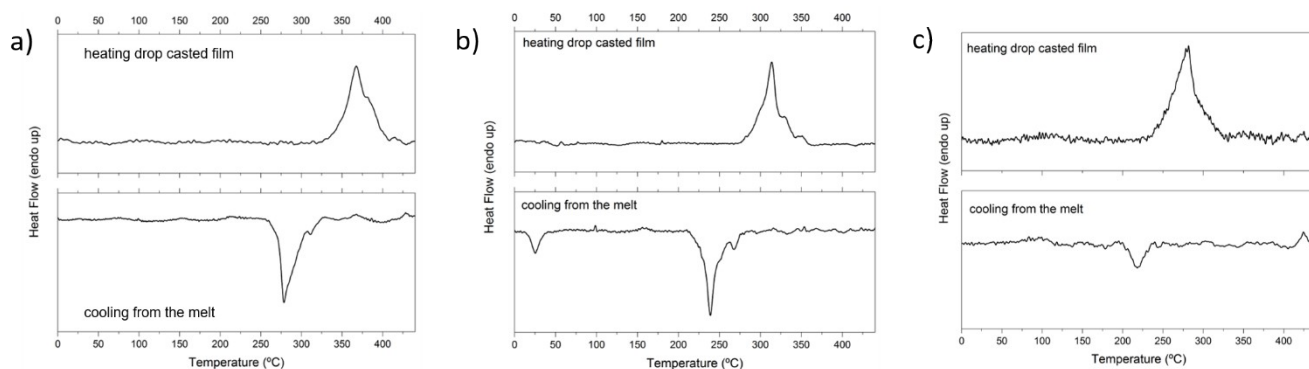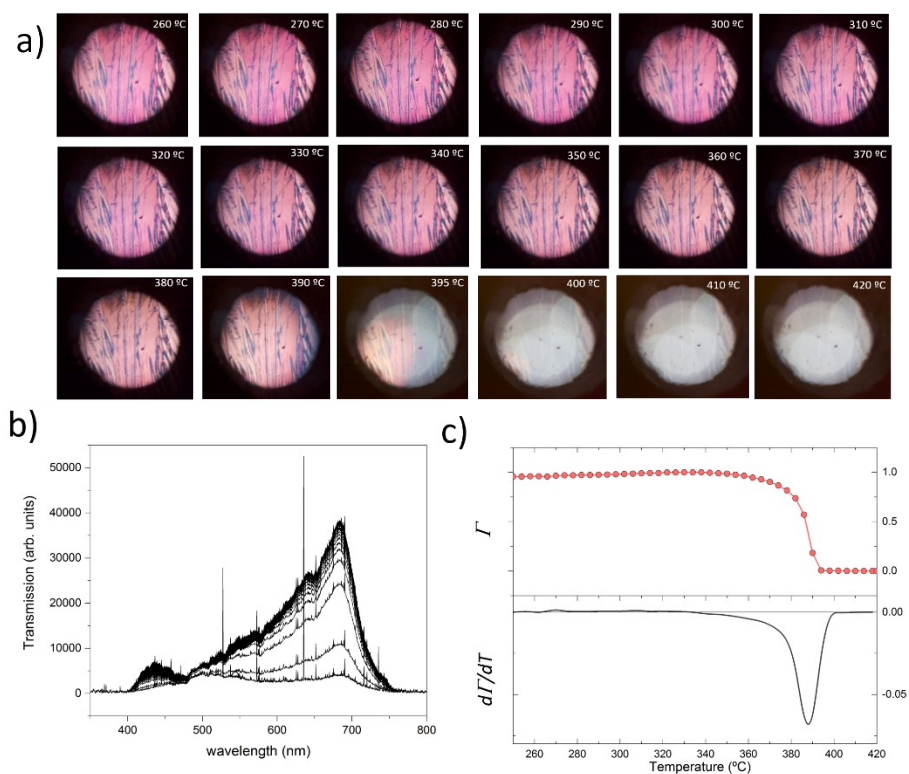
Figure S4. FSC 1st heating and1st cooling scans collected at 2000 °C/sec of HD (a), OD (b) and DT (c) thin films
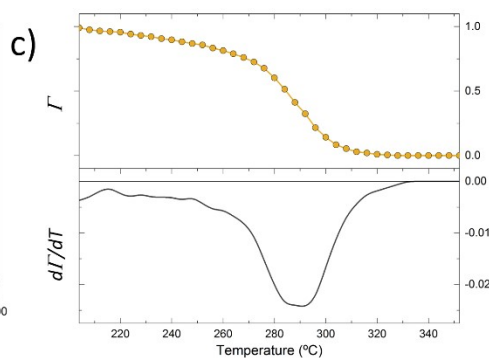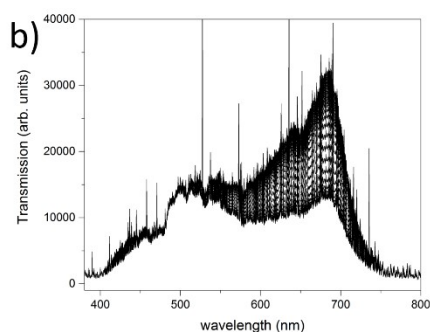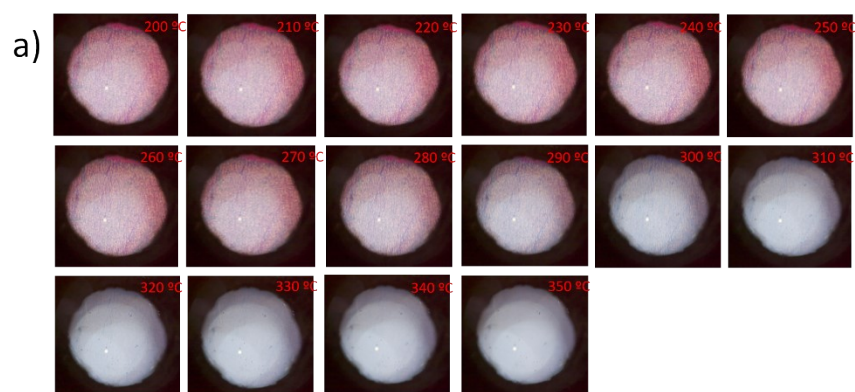
Figure S5: Polarized microscopy (POM-S) experiments. POM-S analysis of the melting behavior of PNDI-T2, DT derivative, thin films. (a) POM images of DT derivative thin film at the temperatures indicated on the top-right part of the images. (b) shows the transmittance spectra recorded as heating during the phase transitions as increasing the temperature. The advance of the normalized integral value of the transmitted light intensity Γ is plotted in (c) against the temperature (top panel). The bottom panel in (c) displays d(Γ)/dT. Heating rate: 4 °C/min. Objective: 10x. Images taken under crossed polarizers.
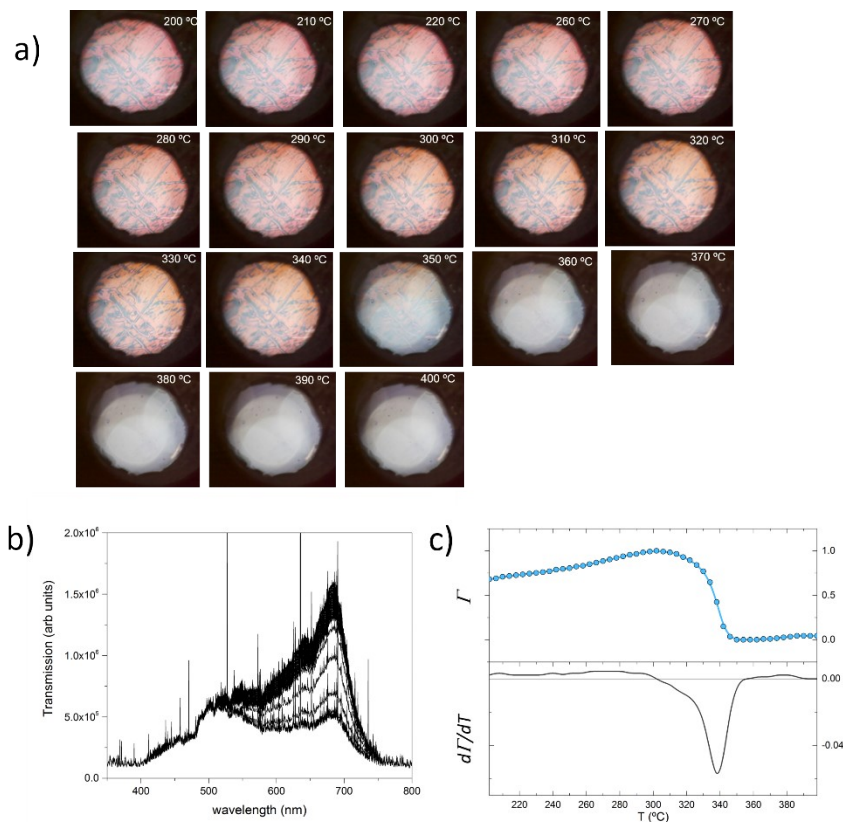
Figure S6: Polarized microscopy (POM-S) experiments. POM-S analysis of the melting behavior of PNDI-T2, OD derivative, thin films. (a) POM images of OD derivative thin film at the temperatures indicated on the top-right part of the images. (b) shows the transmittance spectra recorded as heating during the phase transitions as increasing the temperature. The advance of the normalized integral value of the transmitted light intensity Γ is plotted in (c) against the temperature (top panel). The bottom panel in (c) displays d(Γ)/dT. Heating rate: 4 ºC/min. Objective: 10x. Images taken under crossed polarizers.
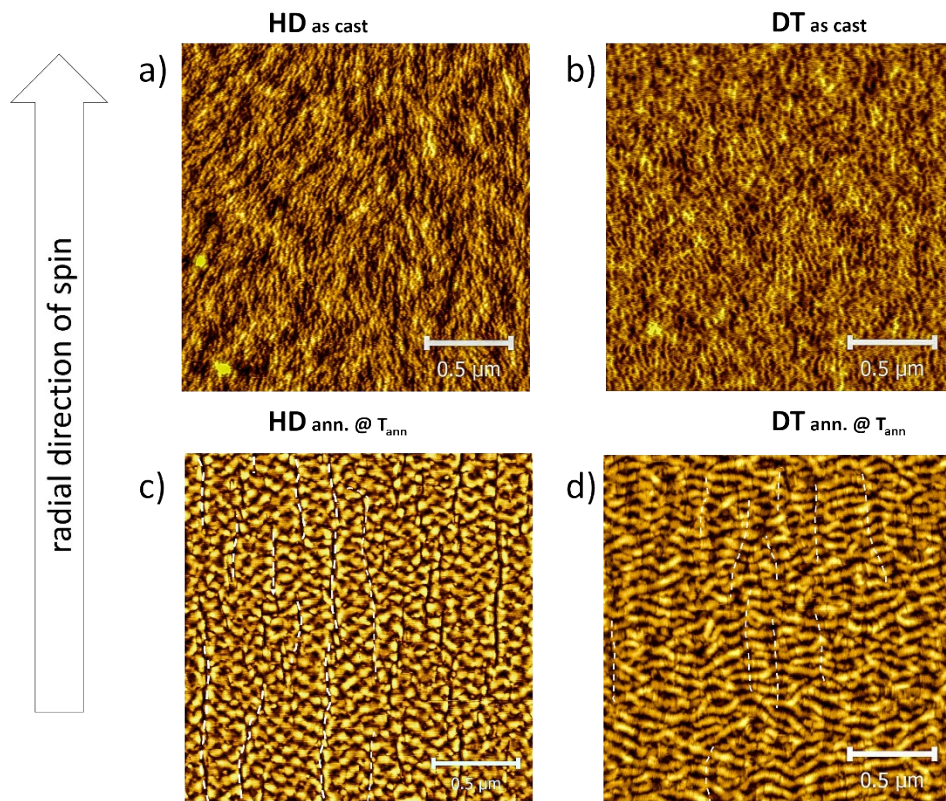
Figure S7: Polarized microscopy (POM-S) experiments. POM-S analysis of the melting behavior of PNDI-T2, HD derivative, thin films. (a) POM images of HD derivative thin film at the temperatures indicated on the top-right part of the images. (b) shows the transmittance spectra recorded as heating during the phase transitions as increasing the temperature. The advance of the normalized integral value of the transmitted light intensity Γ is plotted in (c) against the temperature (top panel). The bottom panel in (c) displays d(Γ)/dT. Heating rate: 4 ºC/min. Objective: 10x. Images taken under crossed polarizers.

Figure S8: AFM analysis. Tapping Mode Atomic Force Microscopy topography images of HD (a,c) and DT (b,d) derivatives, as cast (a,b) and after annealing at T_{ann} (c,d).
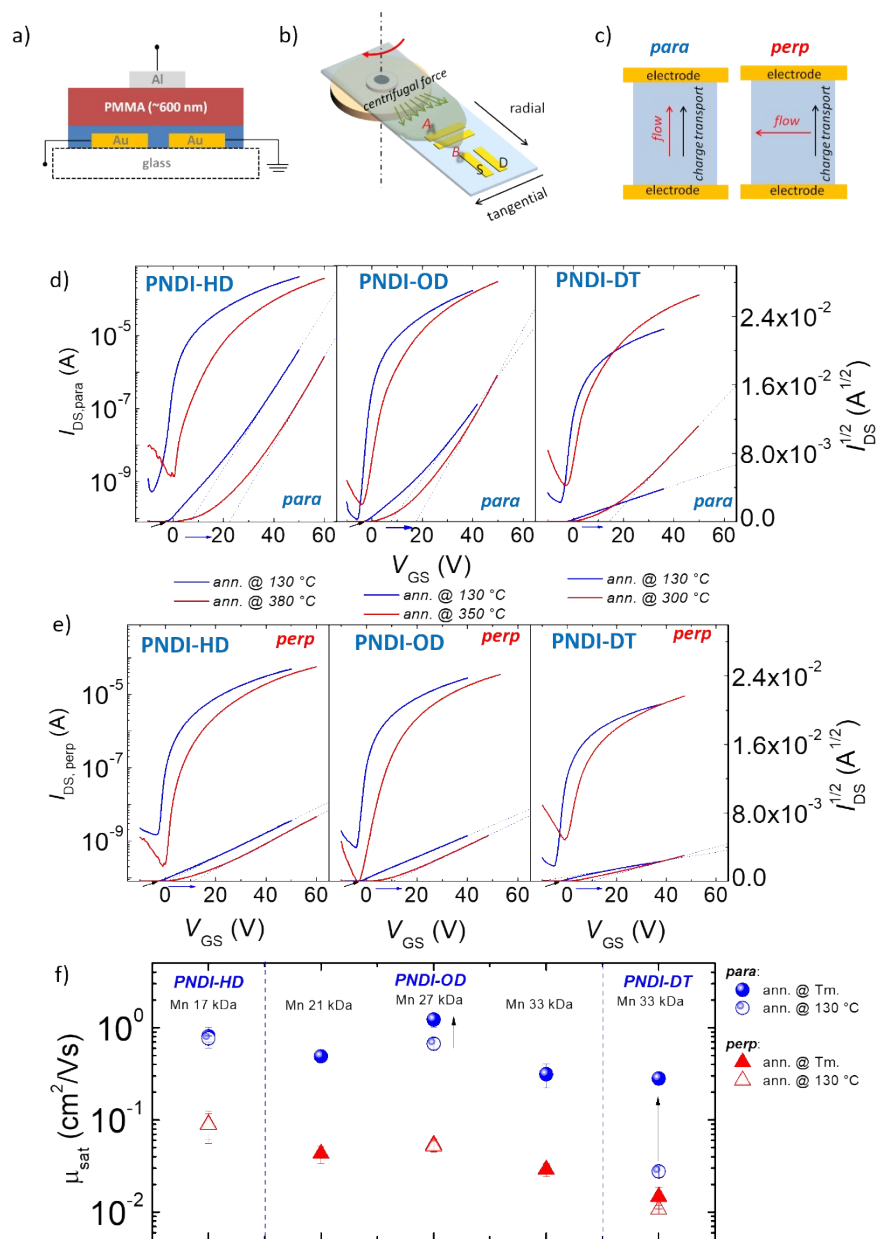
Figure S9. a) Top-Gate, Bottom-Contacts OFETs configuration employed in this work (W= 2000 μm; L = 20 μm; C_{die}= 4.55×10⁻⁵ Fm⁻²); (b) sketch of the off-center spin coating deposition method employed for the deposition of the semiconductors; c) schematic of *para* and *perp* Source & Drain configurations for the extraction of field effect mobility parallel and perpendicular to main molecular backbones orientation; (d,e) representative saturation transfer curves (V_{DS} = 40V) of HD, OD and DT derivatives aligned films after annealing at 130 °C and Tm (380 °C, 350 °C and 300 °C for HD, OD and DT, respectively); (f) summary of saturation mobilities extracted from all the OFETs of this work, including OD batches with variable Mn. **See Appendix B for non-ideality analysis.**
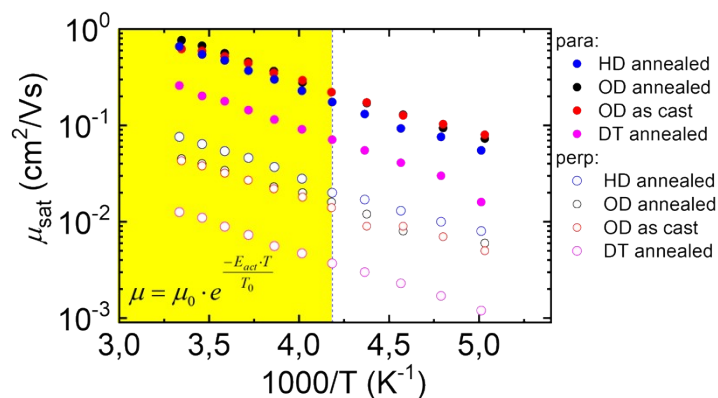
Figure S10. Variable Temperature OFET analysis. OFETs saturation mobility values at variable operating temperatures; Arrhenius equation for activation energy (E_{act}) extraction is also reported. Invariant activation energy values can be extracted at each condition. We mainly address the invariant activation energy to the strong intramolecular charge localization characterizing PNDI-T2 systems: charge transfer energy barrier is solely sized by the intramolecular reorganization energy, in these molecular systems invariant due to the locked molecular conformation. Basing on this statement, it follows that: 1) short range re-arrangement upon annealing has no influence on activation energy since charge transfer energy barrier is solely sized by intramolecular reorganization energy; 2) the long-range molecular alignment, effective in sizing mobility, has no influence on activation energy, since it affect mobility not by sizing the energetic of charge transfer events but by sizing the percolation paths, i.e. the number of effective charge transfer events due for each percolation cluster (as schematized in Figure 5b,c).
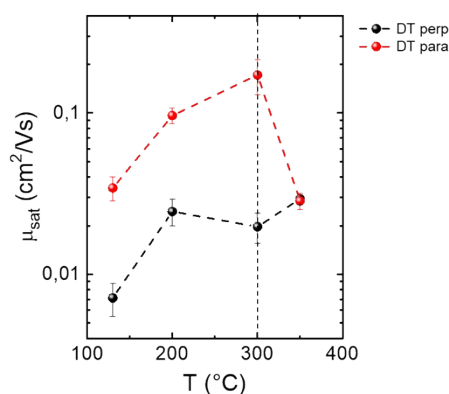
Figure S11. Summary of saturation mobilities extracted from DT OFETs, both in parallel and perpendicular directions of transport, at variable temperatures.

Appendix A: GIWAXS Analysis

The GIWAXS measurements were taken at beamline 11-3 at the Stanford Synchrotron Radiation Lightsource at SLAC, and the image data was processed using the python packages pyfai and pygix. The image is then converted into a reciprocal space map (Figure S9) after being calibrated with a LaB6 reference sample. To get the 1-dimensional q data, the image is converted to q- χ space, multiplied by $\sin(\chi)$ to correct for GIWAXS geometry, and then integrated over χ to produce sector slices. The out-of-plane line cuts, which contain lamellar information, is represented by $\chi = 80\text{-}90°$, and the in-plane line cuts, which contain backbone and $\pi\text{-}\pi$ information, is $\chi = 0 - 10°$.

To extract the crystallite size and paracrystalline disorder for the (100) and (001) peaks, we used the Williamson-Hall method.[3] This method estimates crystallite size (Lc) and paracrystalline disorder (g) from the peak width:

$$\left(\frac{(\Delta_q)_{hkl}}{2\pi}\right)^2 = \left\{(1/L_c)^2\right\}_{\text{intercept}\,(m=0)} + \left\{\frac{(\pi g)^4}{d_{hkl}{}^2}\right\}_{\text{slope}} m^4$$

Where $(\Delta q)hkl$ is the FWHM for the peak (hkl) when plotted in Intensity vs q, Lc is the crystallite size, g is the paracrystalline disorder, dhkl is the corresponding d-spacing of the (hkl) peak, and m is the diffraction order of the peak. The FWHM is taken from a Least-Squared-Error fit of the 1D line cut, with the peaks fitted to a Lorentzian. This method is reliably done for the (100) and (001) peaks due to the presence of multiple orders of highly defined peaks (see Figure S9). However, in the $\pi\text{-}\pi$ stacking direction, only a single peak is observed. An estimate for crystallite size is then given by Scherrer's Equation:
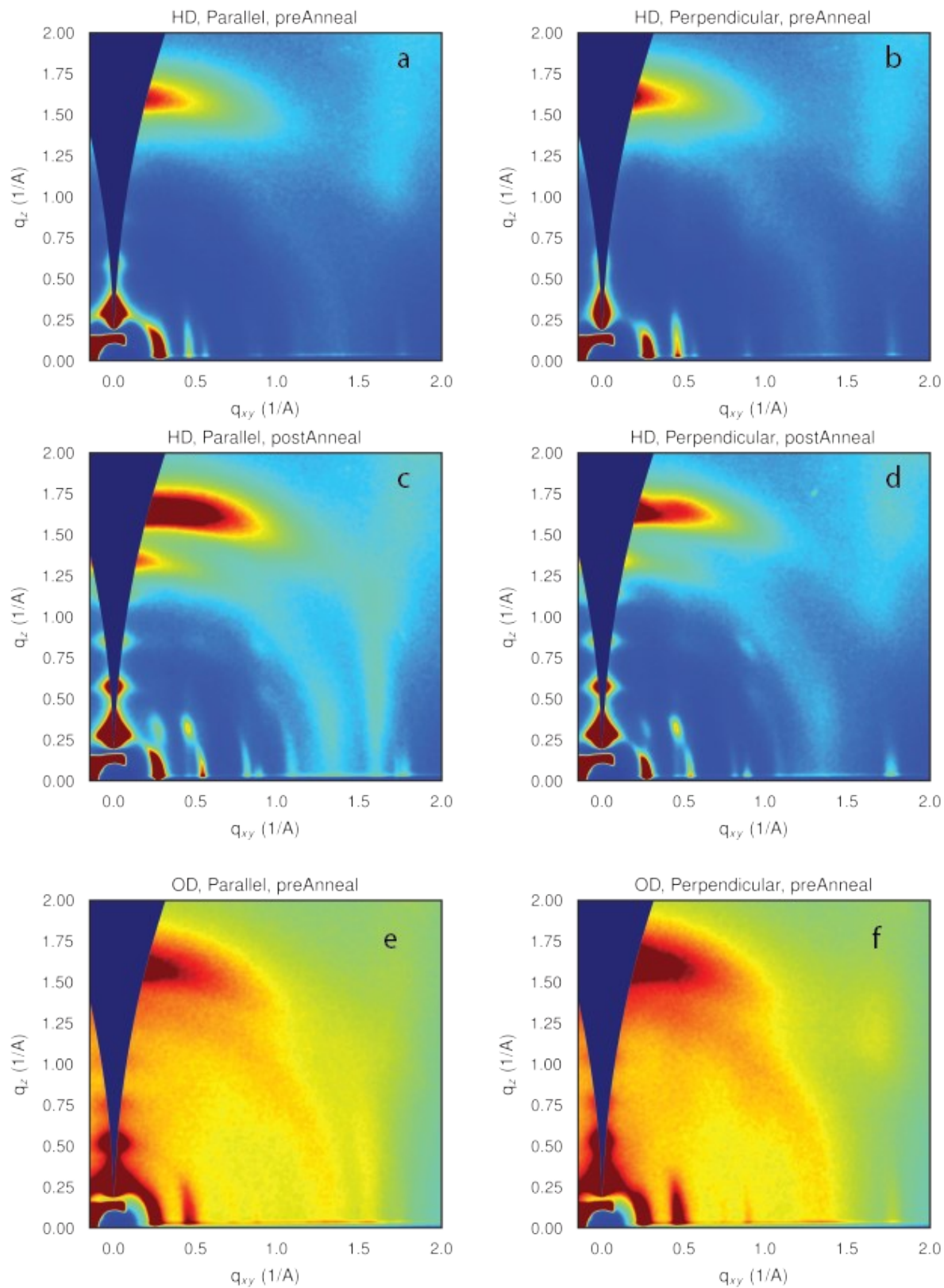
$$L_c = \frac{2\pi K}{\Delta_q}$$

Where we use shape factor $K \approx 0.9$. An estimate for paracrystalline disorder with a single peak can be obtained:[4, 5]

$$g = \sqrt{\frac{\Delta_q}{2\pi q_0}}$$

The latter estimate assumes that peak-width is entirely dominated by paracrystalline disorder, as opposed to the Scherrer's Equation, which assumes that the peak width is entirely dominated by crystallite size.

$$L_c = \frac{d_{hkl}}{2\pi g^2}$$

Eqn (3) has been shown by Noriega, et al. to be a reliable, if conservative, estimate of polymer π-stacking paracrystallinity,[5] and the corresponding crystallite size is then estimated[4] with

OD, Parallel, postAnneal

OD, Perpendicular, postAnneal

DT, Parallel, preAnneal

DT, Perpendicular, preAnneal

DT, Parallel, postAnneal

DT, Perpendicular, postAnneal
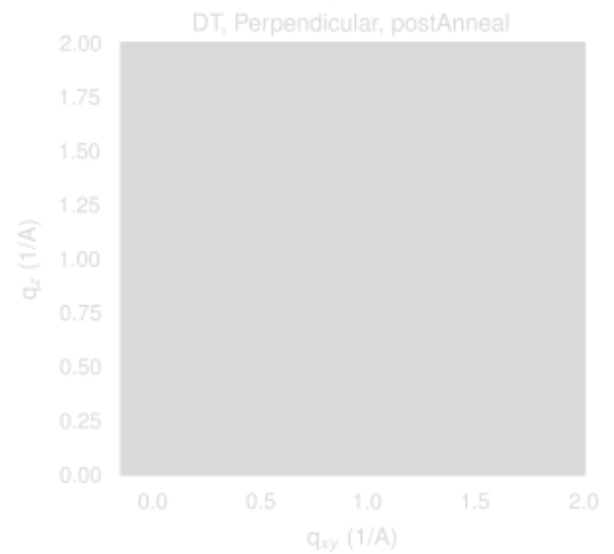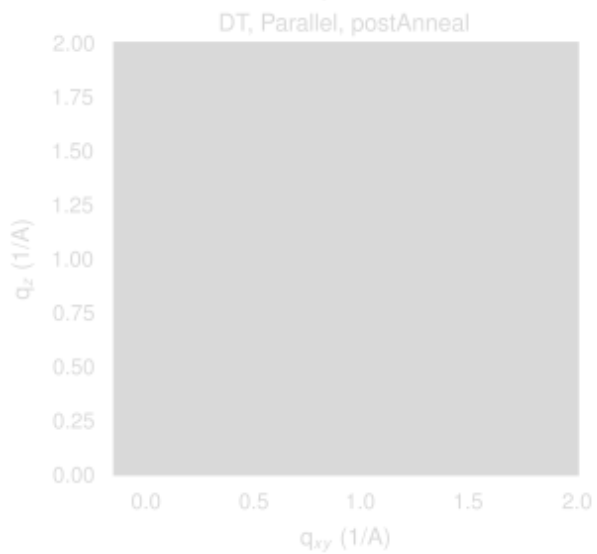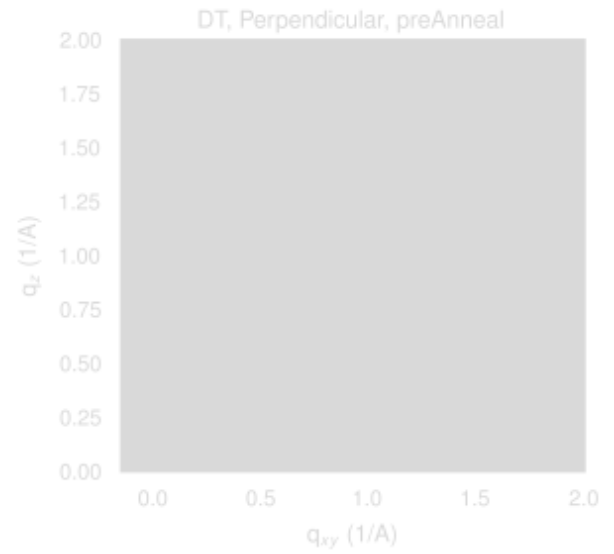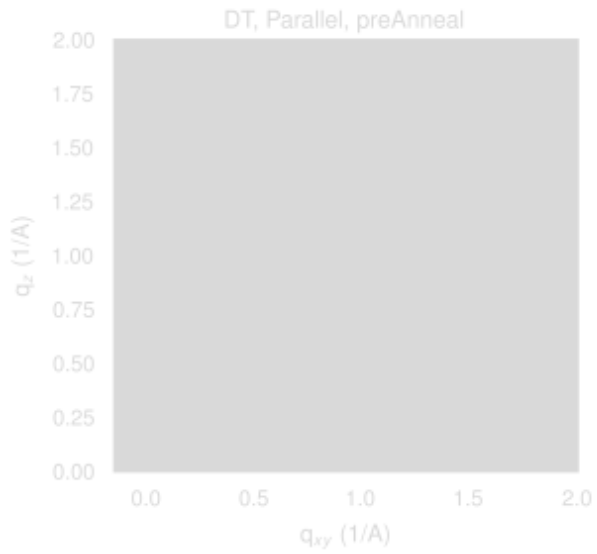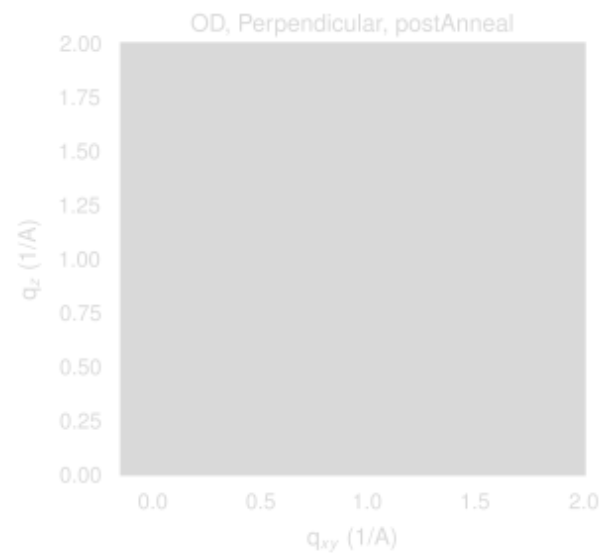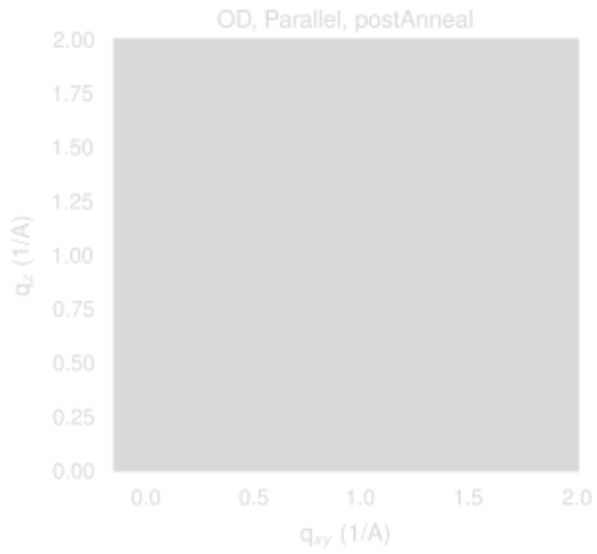
Figure S12. GIWAXS Images taken for each sidechain derivative. For the HD sidechains: (a) before annealing along the coating direction; (b) before annealing, perpendicular to the coating direction; (c) after annealing, parallel to the coating direction; and (d) after annealing, perpendicular to the coating direction. For the OD sidechains: (e) before annealing along the coating direction; (f) before annealing, perpendicular to the coating direction; (g) after annealing, parallel to the coating direction; and (h) after annealing, perpendicular to the coating direction. For the DT side chains: (i) before annealing along the coating direction; (j) before annealing, perpendicular to the coating direction; (k) after annealing, parallel to the coating direction; and (l) after annealing, perpendicular to the coating direction.

	hkl (alignment)	D-spacing, (Å)			Coherence Length (nm)			Paracrystalline Disorder, g		
		As cast	Annealed @ Tann		As cast	Annealed @ Tann	Tann/ As cast	As cast	Annealed @ Tann	Tann /As cast
HD	010 ($\parallel$)	3.96	3.91		3.0	4.8	1.6	0.145	0.114	0.78
	100 ($\perp$)	22.6	21.8		5	13	1.6	0.256	0.065	0.24
	001' ($\perp$)	7.1	7.1		7	15	2.1	0.044	0.044	1
OD	010 ($\parallel$)	3.99	3.97		3.9	4.2	1.05	0.127	0.123	0.97
	100 ($\perp$)	23.9	23.5		21	27	1.3	0.149	0.069	0.46
	001' ($\perp$)	7.0	7.1		11	18	1.6	0.044	0.039	0.9
DT	010 ($\parallel$)	3.92	3.99		6.2	6.2	1.0	0.100	0.101	1.01
	100 ($\perp$)	25.6	25.2		8	35	4.23	0.125	0.066	0.54
	001' ($\perp$)	7.0	7.1		7	17	2.48	0.049	0.038	1.01

Table S2. The extracted d-spacings, crystallite sizes, and paracrystalline disorders, before and after thermal annealing for each sidechain derivative.

Appendix B: OFETs non-ideality analysis

Table S3. Summary of mean threshold voltage (V_{Th}) values extracted from PNDI-T2 based OFETs, as cast and after annealing at T_{ann}

	HD para	HD perp	OD para	OD perp	DT para	DT perp
As cast	$V_{Th}=7\pm1V$	$V_{Th}=2\pm2V$	$V_{Th}=7\pm2V$	$V_{Th}=-3\pm1V$	$V_{Th}=-3\pm2V$	$V_{Th}=-7\pm4V$
T_{ann}	$V_{Th}=22\pm2V$	$V_{Th}=12\pm2V$	$V_{Th}=17\pm2V$	$V_{Th}=6\pm2V$	$V_{Th}=10\pm5V$	$V_{Th}=7\pm3V$
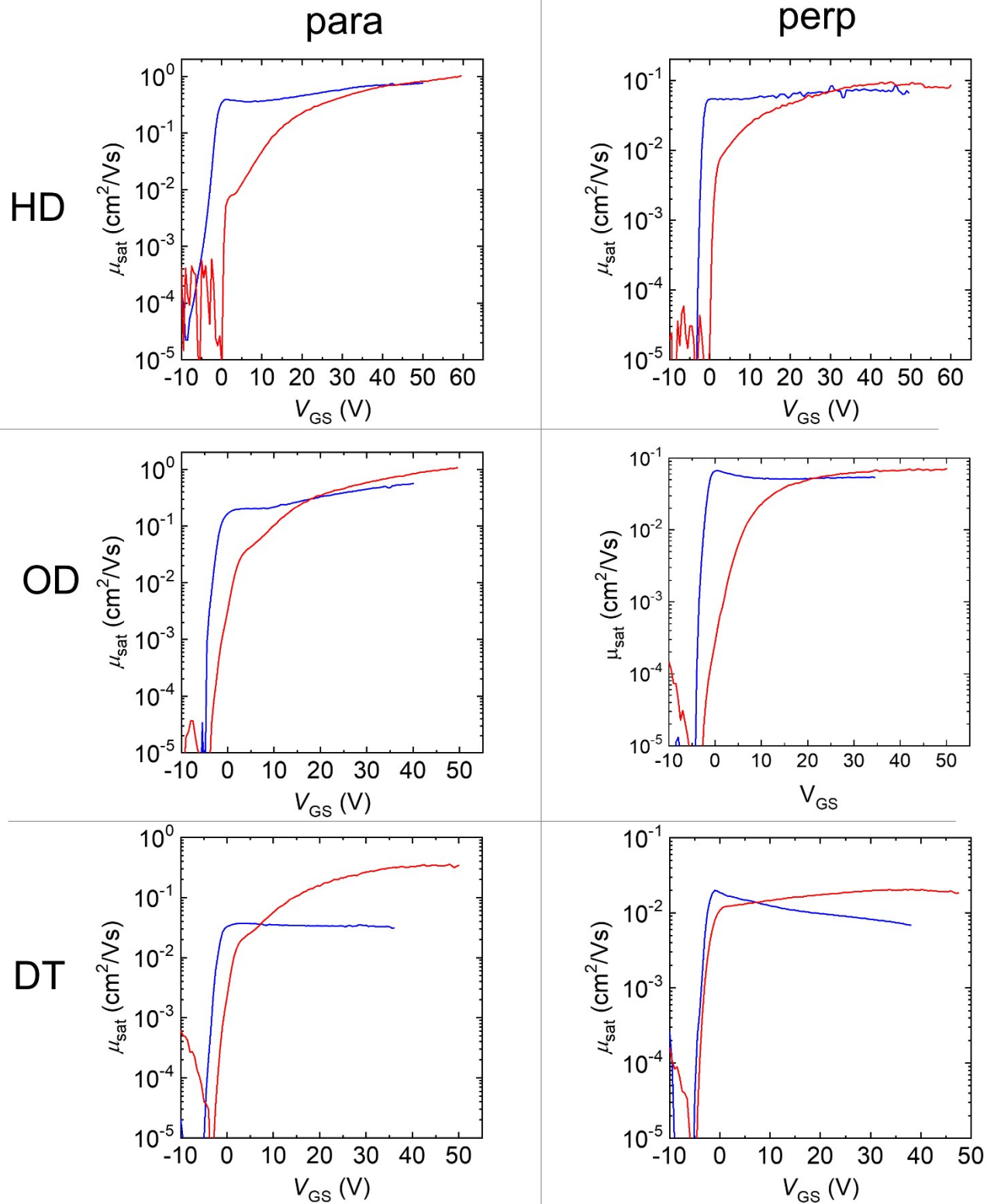
Figure S13. Plots of effective saturation mobility (μ_{sat}) vs. gate voltage (V_{GS}) of all OFETs characteristics reported in Figure S9d-e (blue curves: PNDI-T2 as cast; red curves PNDI-T2 annealed at T_{ann}). The V_{GS}

dependent values of μ_{sat} were obtained from the slope of I_{DS} vs. V_{GS} ($I_{DS}^{0.5}$ vs. V_{GS}) of figure S9d-e, calculated every three points around each V_{GS} value.

1.   Steyrleuthner, R.; Schubert, M.; Howard, I.; Klaumünzer, B.; Schilling, K.; Chen, Z.; Saalfrank, P.; Laquai, F.; Facchetti, A.; Neher, D., Aggregation in a high-mobility n-type low-bandgap copolymer with implications on semicrystalline morphology. *Journal of the American Chemical Society* **2012,** *134* (44), 18303-18317.
2.   Luzio, A.; Criante, L.; D'innocenzo, V.; Caironi, M., Control of charge transport in a semiconducting copolymer by solvent-induced long-range order. *Scientific reports* **2013,** *3* (1), 1-6.
3.   Abdelsamie, M.; Toney, M. F., Microstructural Characterization of Conjugated Organic Semiconductors by X-Ray Scattering. *Conjugated Polymers: Properties, Processing, and Applications* **2019**, 62.
4.   Rivnay, J.; Noriega, R.; Kline, R. J.; Salleo, A.; Toney, M. F., Quantitative analysis of lattice disorder and crystallite size in organic semiconductor thin films. *Physical Review B* **2011,** *84* (4), 045203.
5.   Noriega, R.; Rivnay, J.; Vandewal, K.; Koch, F. P.; Stingelin, N.; Smith, P.; Toney, M. F.; Salleo, A., A general relationship between disorder, aggregation and charge transport in conjugated polymers. *Nature materials* **2013,** *12* (11), 1038-1044.